geotechnics

Article

Laboratory-Based Correlation between Liquefaction Resistance and Shear Wave Velocity of Sand with Fines

Anthi I. Papadopoulou * and Theodora M. Tika

Laboratory of Soil Mechanics, Foundations and Geotechnical Earthquake Engineering, Department of Civil Engineering, Aristotle University of Thessaloniki, 541 24 Thessaloniki, Greece; tika@civil.auth.gr
* Correspondence: anthipap@civil.auth.gr

Abstract: This paper presents the results of a laboratory investigation into the effect of non-plastic fines on the correlation between liquefaction resistance and the shear wave velocity of sand. For this purpose, undrained stress-controlled cyclic triaxial and bender element tests were performed on clean sand and its mixtures with non-plastic silt. It is shown that the correlation between liquefaction resistance and shear wave velocity depends on fines content and confining effective stress. Based on the test results, correlation curves between field liquefaction resistance and overburden stress corrected shear wave velocity for sand containing various contents of fines are derived. These curves are compared to other previously proposed by field and laboratory studies.

Keywords: shear wave velocity; bender element; liquefaction resistance; sand; non-plastic; fines

check for updates

Citation: Papadopoulou, A.I.; Tika, T.M. Laboratory-Based Correlation between Liquefaction Resistance and Shear Wave Velocity of Sand with Fines. *Geotechnics* **2021**, *1*, 219–242. https://10.3390/geotechnics1020012

Academic Editor: Wen-Chieh Cheng

Received: 26 July 2021
Accepted: 8 September 2021
Published: 26 September 2021

Publisher's Note: MDPI stays neutral with regard to jurisdictional claims in published maps and institutional affiliations.

Copyright: © 2021 by the authors. Licensee MDPI, Basel, Switzerland. This article is an open access article distributed under the terms and conditions of the Creative Commons Attribution (CC BY) license (https://creativecommons.org/licenses/by/4.0/).

1. Introduction

The velocity of shear wave propagation, V_s, is a key soil property, used for soil characterisation, such as the estimation of small-strain shear modulus, liquefaction resistance, seismic response, and assessment of the effectiveness of soil improvement methods used in soils, identification of transportation of pollutants in soils, as well as others.

Liquefaction of sandy soils under cyclic loading conditions is considered one of the major causes of damage to earth structures and foundations. To date, a great research effort has been devoted to improving the knowledge concerning the liquefaction characteristics of natural soil deposits and the ability to predict the nature and the extent of the liquefaction phenomenon. In practice, liquefaction resistance is evaluated from laboratory tests such as cyclic simple shear, cyclic triaxial, and cyclic torsional shear, on undisturbed or reconstituted samples and by field tests. Semi-empirical field-based procedures for evaluating the liquefaction potential during earthquakes are based on correlations between field behaviour and in-situ index tests, such as standard penetration test (SPT), cone penetration test (CPT), Becker penetration test (BPT), and shear wave velocity (Vs). Seed et al. (1971) [1] proposed the oldest and perhaps the most widely used procedure termed the "simplified procedure", developed from evaluations of field observations and field and laboratory test data, in which the cyclic stress ratio, CSR = τ_{av}/p'_0, is correlated with the SPT blow counts, corrected for both effective overburden stress and energy, $(N_1)_{60}$, for clean sands and silty sands with fines content greater than 5% and earthquake magnitude, M = 7.5. Through the years the "simplified procedure" has been updated [2] and revised relations for use in current practice have been recommended. Idriss and Boulanger (2004) [3] re-evaluated SPT and CPT case history databases and re-examined the semi-empirical procedures for evaluating the liquefaction potential of saturated cohesionless soils during earthquakes. Cavallaro et al. (2018) [4] determined the shear wave velocity profiles in various areas of the Emilia-Romagna Region, in Italy, by means of a large series of in situ, geophysical and laboratory tests, for the analysis of significant and widespread liquefaction phenomena, observed during the seismic events of May 2012.

The evaluation of liquefaction resistance or cyclic resistance ratio, CRR, based on field evaluation of shear wave velocity, V_s, constitutes a promising alternative procedure compared to the approaches based on penetration-type tests. The correlation between the field CRR, CRR_{field}, and V_{s1}, where V_{s1} is the overburden stress-corrected shear wave velocity, similar to the traditional procedures for modifying standard and cone penetration resistances [5], has been the subject of numerous field and laboratory studies over the last thirty years, as described below.

Tokimatsu and Uchida (1990) [6] proposed a 'best fit' CRR_{field}–V_{s1} curve, which also includes the data presented by [7–9] and is based on a combination of in situ measurements of V_s and laboratory liquefaction tests. Kayen et al. (1992) [10] and Lodge (1994) [11] developed field CRR_{field}–V_{s1} curves for sites that did and did not liquefy during the 1989 Loma Prieta earthquake. Similarly, Robertson et al. (1992) [5] developed a CRR_{field}–V_{s1} curve from field performance data and seismic CPT tests. Andrus and Stokoe (1997, 2000) [12,13] developed semi-empirical liquefaction resistance criteria from field measurements of shear wave velocity (referred to as semi-empirical procedure below). They proposed different CRR_{field}–V_{s1} curves for soils with different fines content, f_c, to separate liquefaction from no-liquefaction zones for a magnitude 7.5 earthquake, Figure 1. According to Andrus and Stokoe (2000), [13] the case history data and the CRR_{field}–V_{s1} curves they presented are limited to relatively level ground sites with average depths of <10 m, uncemented soils of Holocene-age, ground-water table depths between 0.5 and 6m, and V_s measurements performed below the water table. In the following figure, V_{s1}, was obtained from:

$$V_{s1} = V_s \cdot C_N = V_s \cdot \left(\frac{p_a}{\sigma'_v}\right)^{a=0.25} \tag{1}$$

where C_N is a factor to correct measured V_s for overburden stress, p_a is a reference stress equal to 100 kPa, and σ'_v, is the effective overburden stress in Kpa.

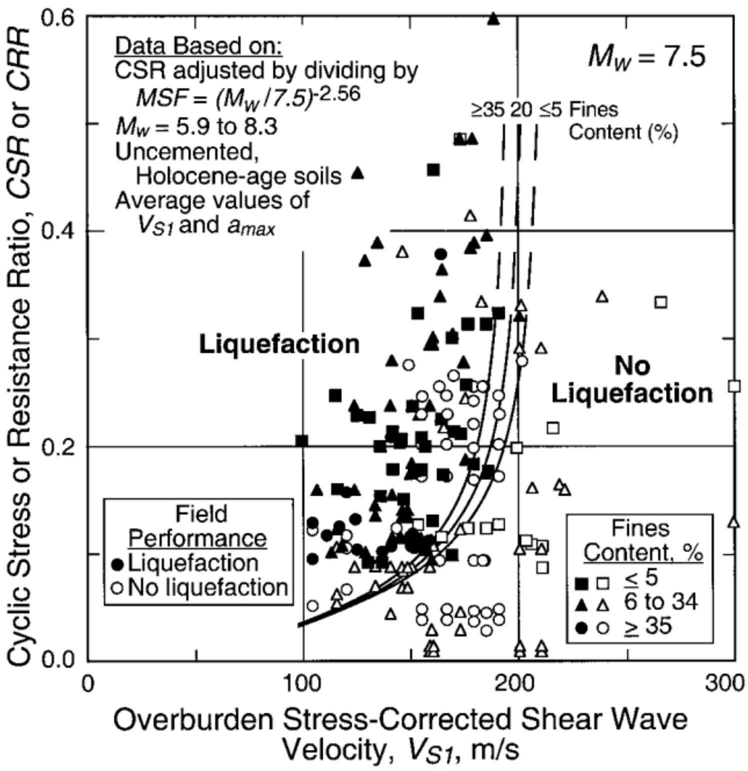

Figure 1. Curves recommended for calculation of CRR from V_{s1} measurements along with case history data [13].

Kayen et al. (2013) [14] reported the results of an 11-year international project to gather 301 new V_s site data from China, Japan, Taiwan, Greece, and the United States and develop probabilistic correlations for seismic liquefaction occurrence in sand with various fines contents. At most sites, a continuous harmonic-wave spectral analysis of surface waves method (SASW) was used for V_s measurement. They noted that the effect of fines is minor in comparison with other aspects of the analysis, namely, the estimation of uncertainty associated with CSR and V_{s1}. They found 14 data points that cross beyond the Andrus and Stokoe (2000) [13] clean sand curve into a frontier previously deemed non-liquefiable and suggested that the concept of a limiting upper bound V_{s1} of 215 m/s for seismic soil liquefaction is unconservative.

Laboratory-based CRR_{field}–V_{s1} correlations have been presented by [15–24], Table 1. These refer to clean sand and sand–silt mixtures with fines content, f_c, up to 75%. In all the above studies, V_s was measured by bender element tests, except for the study by Askari et al. (2011) [21] in which torsional resonant column tests were used, while CRR was estimated from the results of cyclic triaxial tests.

The aim of this work is the investigation of the effect of fines on CRR_{field}–V_{s1} correlation by means of laboratory tests. For this purpose, a parametric laboratory investigation was conducted by means of bender element and undrained cyclic triaxial tests for the measurement of V_s and CRR, respectively, on clean sand and its mixtures with a non-plastic (NP) silt. The test results allow the derivation of CRR_{field}–V_{s1} correlation curves for the sand and the sand–silt mixtures and their comparison with previously proposed curves in the literature, as described above. The V_s measurements are also used for the estimation of the small-strain shear modulus, G_{max}, of the soils, a key parameter for site characterisation, understanding soil behaviour, and the development of soil behaviour models.

Table 1. Laboratory investigations on CRR_{field}–V_{s1} correlation for clean sand and sand with fines.

No	Reference	Soil Type	f_c %	D_{50} mm	D_{10} mm	C_u	e_{max}	e_{min}	Test [1,2]	Liquefaction Criterion	V_s to V_{s1} Conversion	CRR_{lab} to CRR_{field} Conversion
1.	[15]	Maio Liao Sand (MLS) [3]	0	0.11	0.05	2.2	1.130	0.650	BE and CTX MT	5% DA axial strain in 20 cycles	$V_{s1} = V_s$ $\sigma'_h = \sigma'_v = p_a = 100$ kPa	$CRR = \left(\frac{1+2K_0}{3}\right)CRR_{CTX} = \frac{2}{3}CRR_{CTX}$
		Mai Liao Sand (MLS) + fines	15	-	-	-	1.060	0.590				
			30	-	-	-	1.210	0.590				
2.	[16]	Yuan Lin Soils (YLS)	18	0.18	0.035	5.6	1.290	0.850	BE and CTX MT WS L	»	»	»
			43	0.082	0.009	11.1	1.270	0.860				
			89	0.027	0.002	14.4	1.690	1.010				
3.	[17,18]	Kao Hsiung Soils (KHS)	5	0.31	0.13	2.7	-	-	BE and CTX G-P	»	»	»
			21	0.114	0.059	2.2		-				
			22	0.108	-	-	-					
			61	0.052	0.009	8.4	-	-				
4.	[19,20]	Toyoura sand [4]	0	0.16	0.10	1.8	0.970	0.630	BE and CTX ST	5% DA axial strain in 15 cycles	$V_{s1} = V_s\left(\frac{1+2K_0}{3}\right)^{0.25}\left(\frac{p_a}{\sigma'_m}\right)^{0.25}$	$CRR = r_c\left(\frac{1+2K_0}{3}\right)CRR_{CTX}$
		Fuzhoo sand [3]	0	0.32	0.13	3.0	0.790	0.430				
		Tianjin sand [4]	3.7	0.15	0.10	1.7	1.100	0.590				
5.	[21]	Firoozkooh Sand [5]	0	0.25	0.16	1.75	0.870	0.580	TS-RC and CTX MT	initial liquefaction or 5% DA axial strain (whichever occurred first)	$V_{s1} = V_s\left(\frac{1+2K_0}{3}\right)^{0.25}\left(\frac{p_a}{\sigma'_m}\right)^{0.25}$ $K_0 = 1 - sin\varphi'$	$CRR_{field} = \alpha\beta CRR_{CTX}$ $\alpha = K_0 \rightarrow$ *Seed & Peacock*, 1971 $\alpha = \frac{1+2K_0}{3} \rightarrow$ *Seed & Peacock*, 1971 $\alpha = \frac{1+2K_0}{2} \rightarrow$ *Finn et al.*1971 $\alpha = \frac{2(1+2K_0)}{3\sqrt{3}} \rightarrow$ *Castro* 1976 $\alpha = \alpha_{mean}$ [6] $D_r \leq 45\% \rightarrow \beta = 1.15$ $D_r > 45\% \rightarrow \beta = 0.01D_r + 0.7$
		Firoozkooh Sand + Firoozkooh silt	15	0.21	0.02	11.5	0.830	0.410				
			30	0.18	0.01	20	0.854	0.320				
			60	0.047	0.005	28	1.259	0.360				

Table 1. *Cont.*

No	Reference	Soil Type	f_c %	D_{50} mm	D_{10} mm	C_u	e_{max}	e_{min}	Test [1,2]	Liquefaction Criterion	V_s to V_{s1} Conversion	CRR_{lab} to CRR_{field} Conversion
6.	[22]	Babolsar Sand [7]	0	0.24	0.15	1.80	0.825	0.546	BE and CTX MT	R_u = 1 in 15 cycles	$V_{s1} = \left(V_{s,field}\right)\left(\frac{p_a}{\sigma'_v}\right)^{0.25}$	$CRR_{field} = 0.9\left(\frac{1+2K_0}{3}\right)CRR_{CTX}$
7.	[23]	Firoozkooh Sand	0	0.23	0.18	1.32	0.886	0.637	»	»	»	»
		Firoozkooh sand + Firoozkooh silt	3	-	-	-	0.886	0.633				
			5	-	-	-	0.895	0.630				
			15	-	-	-	0.838	0.554				
			25	-	-	-	0.862	0.497				
8.	[24]	F75 sand [8]	0	0.29	0.15	2.13	0.820	0.480	BE and CTX MT	R_u = 1 in 15 cycles	$V_{s1} = (V_{s-lab})(K_0)^n\left(\frac{p_a}{\sigma'_m}\right)^{2n}$ $K_0 = 1 - sin\varphi'$ $n = 0.125$	$CRR_{field} = (0.9)(c_r)(CRR_{CTX})$ $c_r = \frac{2(1+2K_0)}{3\sqrt{3}}$
		F75 sand + Sil-Co-Sil 125 silt	5	0.29	0.13	2.5	0.780	0.420				
			15	0.28	0.033	9.7	0.850	0.360				
			30	0.23	0.013	21.9	0.980	0.300				
			50	0.10	0.007	25.0	1.210	0.400				
			60	0.09	0.006	18.2	1.370	0.450				
			75	0.04	0.005	19.1	1.670	0.560				

[1] BE: Bender element test, CTX: Cyclic Triaxial test, TS-RC: Torsional Resonant Column test. [2] MT = Moist Tamping specimen preparation method, WS = Water Sedimentation, ST = Saturated Tamping, L = Laval sampling undisturbed specimens, G-P = specimens recovered by Gel-push sampler. [3] Angular; [4] Sub-Angular; [5] Sub-Angular to Sub-Rounded. [6] a_{mean} is the mean value of parameter a, calculated from the equations of [25–27]. [7] Sub-Rounded; [8] Rounded.

2. Tested Materials

The materials used in the testing program were natural quartz clean sand (S) with well-rounded grains and its artificial mixtures with non-plastic silt (F), a ground product of natural quartz deposits in Assyros, Greece. Tests were conducted on the clean sand and on three groups of mixtures of the sand with the silt, having fines content, f_c, of 15, 25, and 35% of the total dry mass of mixtures (noted as S, SF15, SF25, and SF35, respectively). A more detailed description of the mixtures is presented in [28].

The physical properties and grain size distributions of the tested materials are presented in Table 2 and Figure 2, respectively.

Table 2. Physical properties of tested material.

Soils	G_s	D_{50} (mm)	C_u	f_c (% < 75μm)	e_{min}	e_{max}
Sand (S)	2.649	0.30	1.3	0	0.582	0.841
Silt (F)	2.663	0.02	7.5	100	0.658	1.663
SF15	2.651	0.30	8.8	15	0.380	0.750
SF25	2.653	0.30	16.8	25	0.350	0.686
SF35	2.654	0.27	24.6	35	0.345	0.777

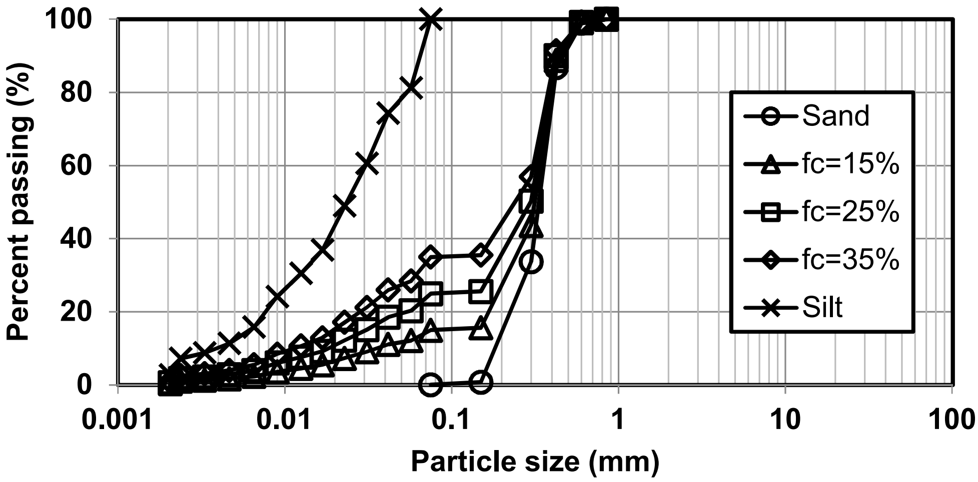

Figure 2. Grain size distributions of the materials tested.

3. Testing Procedure

As stated previously, the testing program comprised bender element and undrained stress-controlled cyclic triaxial tests for the determination of V_s and CRR of the tested materials, respectively. Both types of tests were performed using a closed-loop automatic cyclic triaxial apparatus, designed and manufactured by MTS (Material Test Systems Corporation, Eden Prairie, MN, USA) [28]. Its principle of operation is based on the cooperation of its two main systems, the servo-hydraulic and the electronic, with the application of closed-loop control, firstly, for either the stress or the strain control of the actuator rod, and, secondly, for the control of the pressure inside the triaxial cell.

3.1. Specimen Preparation

The specimens (height/diameter = 150 mm/100 mm) were formed by moist tamping at a water content varying between 4 and 12% using the undercompaction method, introduced by [29]. Moist tamping was preferred to other preparation methods, such as pluviation techniques, in order to achieve uniform density and homogeneous distribution of fine particles and to enable the formation of loose specimens, as moist tamping produces specimens of varying densities [30]. Saturation was achieved by percolating through the specimen, from the bottom to the top drainage line, first carbon dioxide gas (CO_2) for 20 min and then de-aired water. A suction pressure of 15 kPa was applied while dismantling the specimen, measuring its dimensions, and assembling the triaxial cell. In order to ensure full saturation, a series of steps of simultaneous increasing cell pressure and back pressure were performed, while maintaining effective confining stress of 15 kPa. A final back pressure of 200–400 kPa was found to be sufficient, as the parameter of pore water pressure, $B = \Delta u/\Delta\sigma$, did not increase by further increasing back pressure. In all the tests the parameter B had values from 0.95 to 1.00. After completion of saturation, the specimens were isotropically consolidated under effective isotropic stress, p'_0, ranging from 50 to 300 kPa. A period of time equal to double the consolidation time of the specimens was allowed before testing. During consolidation, the volume change and the axial displacement of the specimens were recorded in order to calculate the post-consolidation void ratio, e.

3.2. Bender Element Tests

The bender element system was installed in the cyclic triaxial apparatus. The bender elements were encapsulated and then mounted into inserts which were fixed into specially manufactured top and bottom platens of the cylindrical specimen. A function generator (Agilent 33220A) was used for the excitation of the source sensor (top platen) with an electrical signal. Waves transmitted through the soil specimen were recorded at the other end by the bender element in the base pedestal (receiver). A digital oscilloscope (Agilent 54642A) was used for the display and recording of both the input-source and output-receiver signals. The function generator and the oscilloscope were connected to a computer. The type of electrical signal used to drive the source sensor was a sinusoidal pulse of 10 Volts (amplitude) at a frequency, f, ranging from 3 to 10 kHz. An automated measurements system was developed for signal acquisition and analyses which included recording, appropriate filtering, and automated measurement of travel time of the signal in time and frequency domain [31]. In this work, the start-to-start method was used for the measurement of shear wave travel time in the soil specimen [32]. To account for the near field effect disturbances that are believed to be the influence of P wave signals, that reach before the actual shear waves, as well as signal noises, signal arrival was observed by passing waves of different frequencies [33,34]. According to the start-to-start method, when the first amplitude in the time history of the receiver signal matches the direction of input motion (source signal), the point where the receiver signal takes off from the baseline (horizontal line of zero voltage when there is no signal) is the time of shear wave arrival. In case the first amplitude in the time history of the receiver signal does not match the direction of input motion, the point where the receiver signal first transverses towards the input motion direction and intersects the baseline is the time of shear wave arrival. As the bender element test is considered non-destructive, measurements of V_s were performed at various levels of effective mean (isotropic) stress, p'_0, ranging from 30 to 300 kPa. Test details, as well as the results of the V_s measurements, are presented in Table 3 for the sand and the mixtures.

Table 3. Bender element and cyclic triaxial tests results.

f_c (%)	Test	p'_0 (kPa)	e	f (kHz)	V_S (m/s)	ρ (Kg/m^3)	CRR_{15}
0	S-1	30	0.589	10	197.56	2042.24	-
0	S-2	49	0.587	10	227.98	2044.16	0.583
0	S-3	51	0.662	10	205.21	1997.44	0.326
0	S-4	52	0.673	10	192.50	1992.00	0.301
0	S-5	49	0.685	10	178.46	1983.40	0.277
0	S-6	88	0.585	10	256.50	2016.16	0.401
0	S-7	100	0.658	10	236.61	2001.89	0.257
0	S-8	100	0.670	10	225.66	1995.62	0.240
0	S-9	100	0.679	10	215.14	1990.09	0.228
0	S-10	192	0.581	10	324.38	2051.96	0.396
0	S-11	200	0.654	10	294.81	2007.43	0.241

Table 3. *Cont.*

f_c (%)	Test	p'_0 (kPa)	e	f (kHz)	V_S (m/s)	ρ (Kg/m^3)	CRR_{15}
15	SF15-1	50	0.538	10	135.16	2084.06	0.391
15	SF15-2	51	0.565	7	119.33	2054.87	0.339
15	SF15-3	50	0.599	10	122.88	2042.88	0.287
15	SF15-4	51	0.626	8	122.47	2021.19	0.252
15	SF15-5	50	0.646	10	122.73	2005.62	0.230
15	SF15-6	100	0.522	6	164.68	2106.03	0.281
15	SF15-7	100	0.560	8	152.84	2058.26	0.230
15	SF15-8	98	0.587	10	157.65	2058.16	0.201
15	SF15-9	100	0.622	7	150.99	2026.48	0.171
15	SF15-10	99	0.642	8	154.85	2009.71	0.156
15	SF15-11	199	0.504	10	212.23	2131.61	0.280
15	SF15-12	199	0.549	10	195.40	2108.34	0.221
15	SF15-13	200	0.553	10	201.15	2063.30	0.213
15	SF15-14	199	0.619	8	192.14	2029.98	0.140
15	SF15-15	200	0.638	10	196.18	2014.99	0.120
15	SF15-16	300	0.491	10	246.18	2150.25	0.237
15	SF15-17	300	0.504	10	222.05	2171.29	0.219
15	SF15-18 *	300	0.549	10	226.36	2065.70	0.172
15	SF15-19	300	0.615	10	221.51	2035.25	0.125
15	SF15-20	300	0.636	10	224.04	2017.58	0.114
25	SF25-1	50	0.422	3	110.39	2161.83	0.368
25	SF25-2	50	0.472	3	104.08	2122.89	0.285
25	SF25-3	52	0.505	3	103.76	2098.84	0.245
25	SF25-4	100	0.412	6	147.19	2169.99	0.245
25	SF25-5	103	0.454	3	133.23	2136.14	0.211
25	SF25-6	101	0.479	3	137.01	2116.96	0.194
25	SF25-7	200	0.402	5	192.08	2178.76	0.200
25	SF25-8	201	0.446	6	178.94	2142.63	0.178
25	SF25-9	200	0.469	3	176.92	2125.17	0.163
25	SF25-10	300	0.384	6	221.84	2197.82	0.200
25	SF25-11 *	301	0.439	8	209.99	2148.80	0.180
25	SF25-12	302	0.463	6	203.46	2129.53	0.160
35	SF35-1	49	0.428	6	129.24	2158.37	0.178
35	SF35-2	50	0.471	10	108.04	2124.71	0.148
35	SF35-3	51	0.475	7	99.48	2121.15	0.141
35	SF35-4	51	0.485	6	102.87	2114.08	0.133
35	SF35-5	99	0.387	8	163.62	2192.32	0.177
35	SF35-6	98	0.455	5	126.07	2136.80	0.149
35	SF35-7	99	0.456	6	140.17	2136.27	0.149
35	SF35-8	100	0.479	4	127.46	2118.13	0.141
35	SF35-9	200	0.367	9	213.15	2209.52	0.200
35	SF35-10	199	0.441	8	181.61	2148.09	0.145
35	SF35-11	197	0.443	6	173.88	2145.77	0.144
35	SF35-12	200	0.469	8	168.62	2125.64	0.150
35	SF35-13	299	0.334	12	246.27	2239.78	0.237
35	SF35-14 *	299	0.412	7	209.09	2172.55	0.200
35	SF35-15	301	0.432	10	211.53	2155.08	0.191
35	SF35-16 *	301	0.462	8	196.45	2131.10	0.171

* The specimens were subjected to cyclic loading after bender element test.

3.3. Cyclic Triaxial Tests

In the cyclic triaxial tests, the specimens were subjected to a sinusoidally varying axial stress ($\pm\sigma_d$) at a frequency of f = 0.1 Hz under undrained conditions. Typical results of cyclic triaxial tests are presented in Figure 3a,b for sand and a mixture of sand with 15% fines, respectively. Plots of CSR, ε_{DA}, $\Delta u/p'_0$ with time, t and q with ε_{DA} and p', are shown. During cyclic loading, the excess pore water pressure, Δu, builds up and approaches p'_0, when the state of liquefaction is reached ($\Delta u/p'_0 \geq 0.90$). For a given sand, the rate of increase of Δu, its final value and the corresponding double amplitude axial strain, ε_{DA}, depend on p'_0, the density, and the applied cyclic stress ratio, CSR = $\sigma_d/2p'_0$ [28]. The occurrence of ε_{DA} = 5% is customarily used as a reference point to define the state of cyclic softening or liquefaction of both clean sand and sand containing fines [35]. Thus, in order to specify the onset of liquefaction, the number of loading cycles, N, required to reach ε_{DA} = 5%, N_l, is determined by running a series of tests with different CSR values. In view of the typical number of significant load cycles from 10 to 20 (10–20 for an earthquake of a 7.5 magnitude) of actual earthquakes, in this work, the onset of liquefaction and, thus, the cyclic resistance ratio, CRR_{15}, is considered as the CSR required to produce ε_{DA} = 5% in 15 loading cycles.

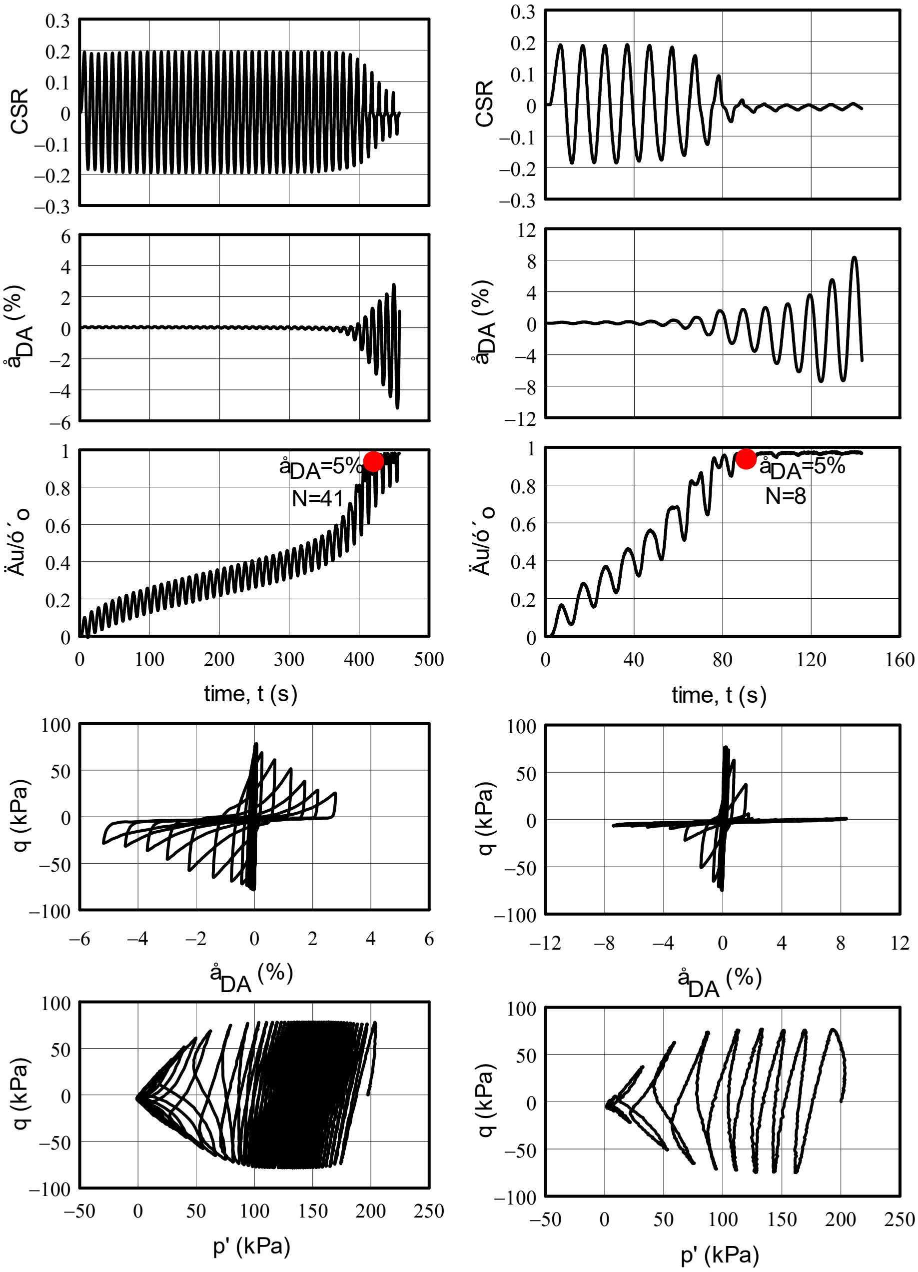

(**a**) (**b**)

Figure 3. The evolution of CSR, ε_{DA}, $\Delta u/p'_0$ with time, t and q with ε_{DA} and p' for a specimen of (**a**) sand (e = 0.663, CSR = 0,20, p'_0 = 200 kPa) and (**b**) sand with 15% fines (e = 0.587, CSR = 0.19, p'_0 = 200 kPa).

Papadopoulou (2008) [28] studied the effect of density, p'_0, and f_c on CRR_{15} of the soils examined in this work and presented a database of results of undrained stress-controlled cyclic triaxial tests on the sand and the sand–silt mixtures with f_c = 15%, 25%, 35%, 40%, and 60%. For each soil type, the V_s value, measured at a given density and p'_0, was correlated with the CRR_{15}, obtained from the above-described database, Table 3. In a few of the tests, CRR_{15} was also measured.

4. Tests Results and Analysis

4.1. Shear Wave Velocity

The variation of V_s with e at various levels of p'_0 is presented in Figure 4. For each tested soil, it is shown that V_s increases with increasing p'_0, and this increase is significantly greater at the transition of p'_0 from 100 kPa to that of 200 kPa. Moreover, for a given p'_0, V_s increases with decreasing e, as shear waves travel faster in denser specimens.

The results of the tests also allow for the estimation of small-strain shear modulus, G_{max}, from V_s from the following equation:

$$G_{max} = \rho \cdot V_s^2 \tag{2}$$

where ρ is the total mass density of the soil.

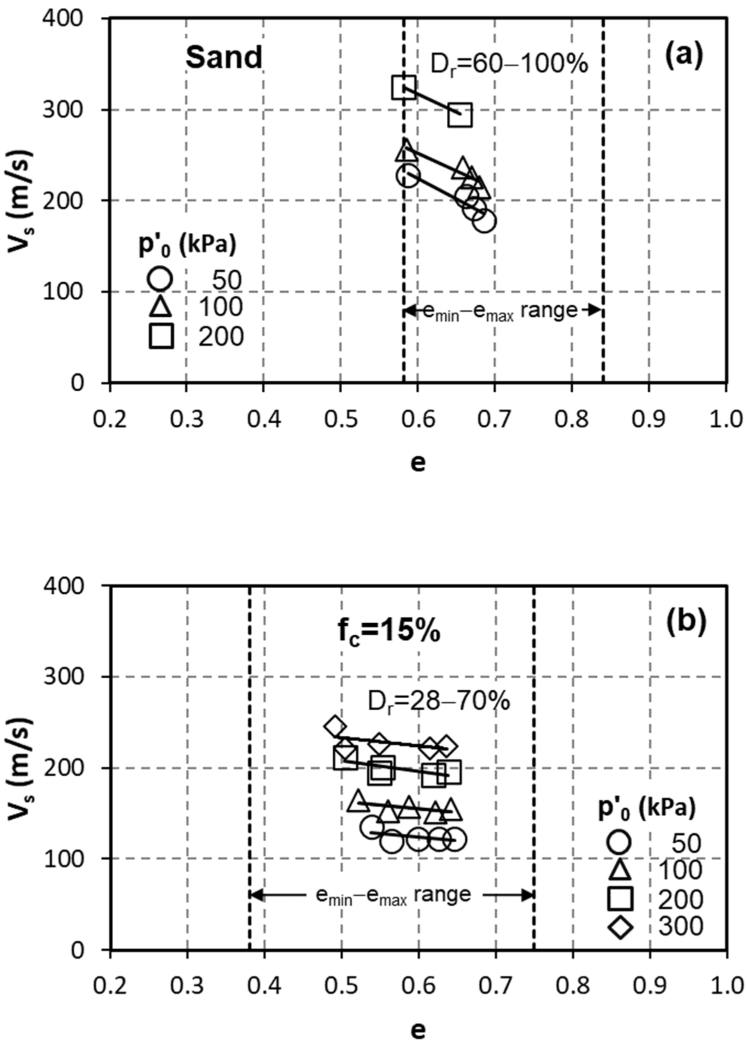

Figure 4. *Cont.*

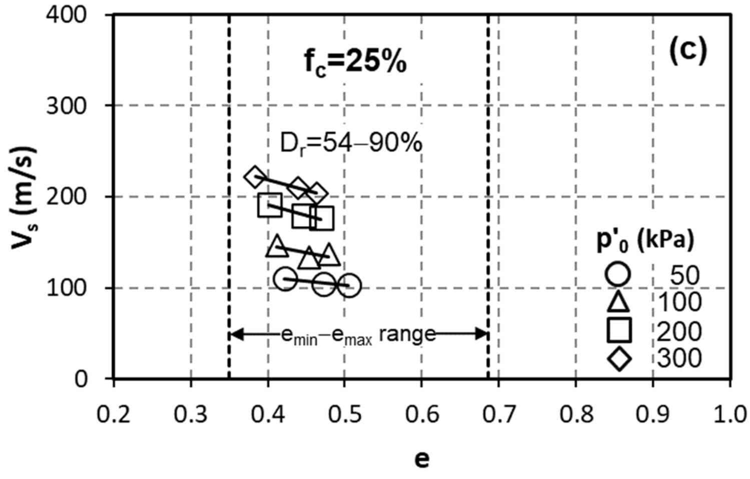

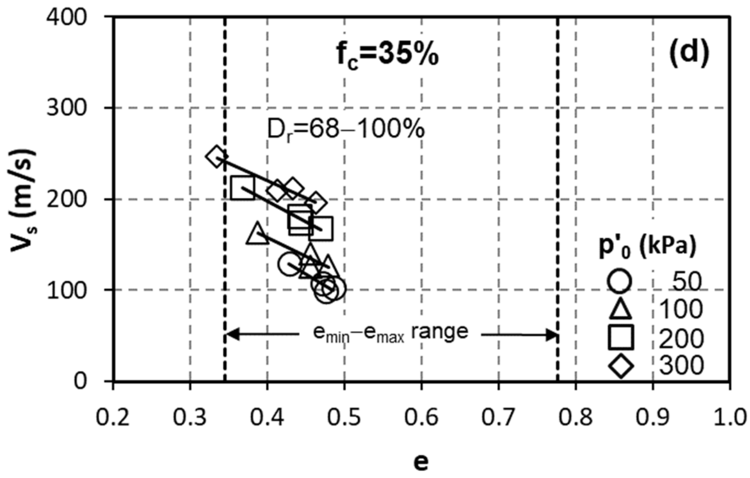

Figure 4. Variation of shear wave velocity, V_s, with void ratio, e, and effective stress, p'_0, for the tested soils, (**a**) sand, (**b**) f_c = 15%, (**c**) f_c = 25% and (**d**) f_c = 35%.

Empirical equations proposed for the estimation of G_{max} of sand are widely used for soil characterisation in common geotechnical engineering practice and constitutive modelling of soil behaviour. Hardin's empirical equation [36], which takes into account the effect of density and effective stress, is the most widely used for the estimation of G_{max}:

$$G_{max} = A \cdot p_a \cdot f(e) \cdot \left(\frac{p'_0}{p_a}\right)^m = A \cdot p_a^{1-m} \cdot e^{-n} \cdot p_0'^{\,m} \tag{3}$$

By combining Equations (2) and (3), V_s can be expressed as follows:

$$V_s = \sqrt{\frac{G_{max}}{\rho}} = \sqrt{\frac{A}{\rho}} \cdot p_a^{\frac{1-m}{2}} \cdot e^{-\frac{n}{2}} \cdot p_0'^{\,\frac{m}{2}} \tag{4}$$

where p_a is reference stress assumed to be 100 kPa, p'_0 is the mean effective stress, $f(e) = e^{-n}$ is the void ratio function [37], and A, m, and n are parameters that depend on soil type.

The values of G_{max} obtained from Equation (2) were used in non-linear regression analysis for the estimation of the parameters A, m, and n in Equations (3) and (4) for the sand and the sand–silt mixtures. The results of this regression analysis are listed in Table 4, while the variation of parameters A and m with f_c is plotted in Figure 5. It is shown that the value of parameter A decreases with increasing f_c, while the value of the stress exponent m for the artificial mixtures is different from the value of 0.5, which is commonly used in practice for clean sand.

Table 4. Values of parameters A, m, and n in Equation (3) for the tested soils.

Soils	e	A (10^3)	m	n	(r^2) *
S	0.581–0.685	381.221	0.545	2.557	0.982
SF15	0.491–0.646	324.693	0.659	0.828	0.980
SF25	0.384–0.505	162.672	0.727	1.162	0.997
SF35	0.334–0.485	109.992	0.625	1.698	0.984

* Coefficient of correlation.

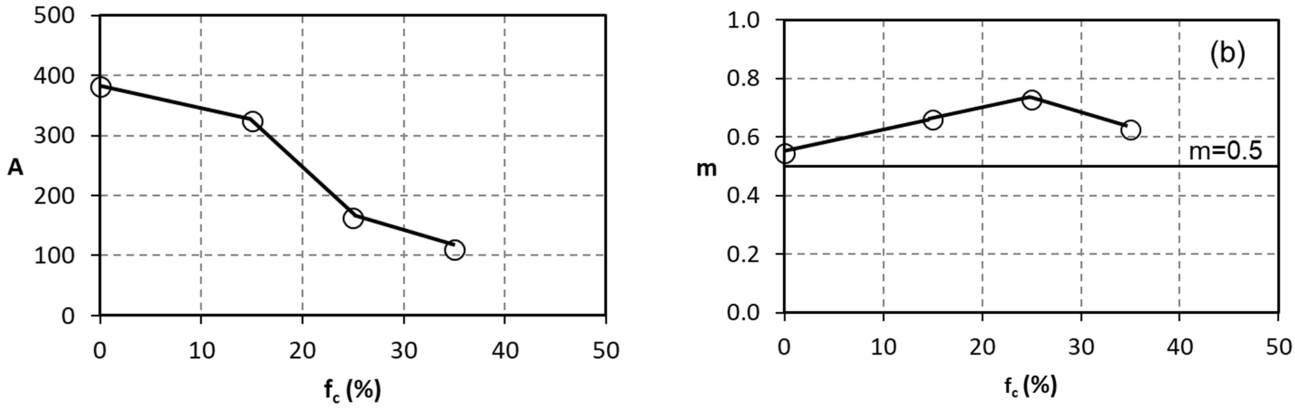

(**a**) (**b**)

Figure 5. Variation of soil dependent parameters (**a**) A and (**b**) m with fines content, f_c (%).

Figure 6 shows normalized G_{max} values of the tested soils with p'_0. To account for the effect of density, G_{max} was normalized by the void ratio function, $f(e) = e^{-n}$, previously determined. It is shown that normalized G_{max} values decrease rapidly with increasing f_c up to 35%.

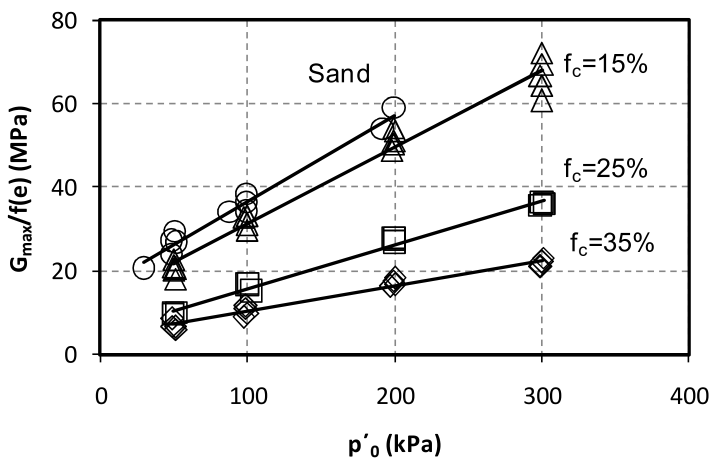

Figure 6. Variation of normalized small-strain shear modulus, $G_{max}/f(e)$, with effective stress, p'_0, for the tested soils.

4.2. Liquefaction Resistance

Figure 7 shows the variation of CRR_{15} with e, at p'_0 = 50, 100, 200, and 300 kPa, for the sand and the sand–silt mixtures, at values of D_r ranging from 7% to 100%. In the following figure, the results for the sand–silt mixtures with f_c = 40% and 60% are also presented [28]. At a given p'_0 and density, CRR_{15} decreases with increasing f_c up to a threshold fines content value, $f_{c,th}$, and increases thereafter with further increasing f_c. For the tested sand–silt mixtures, $f_{c,th}$ is 35% and 25% at p'_0 = 50–200 kPa and 300 kPa, respectively. The behaviour of the mixtures at $f_{c,th}$ is characterised by instability and flow liquefaction. Moreover, it is shown that at a given density, CRR_{15} decreases with increasing p'_0 and that the effect of p'_0 on CRR_{15} diminishes with increasing f_c. The existence of $f_{c,th}$, has also been observed in previous studies on the effect of f_c on the behaviour of sand with fines [38–44]. The $f_{c,th}$ is an important parameter determining the transition from the sand-dominated to the silt-dominated behaviour of mixtures and is related to their particle packing, mean diameter ratio, and separation distance as well as gradation, mineralogy, and particle shape characteristics [45].

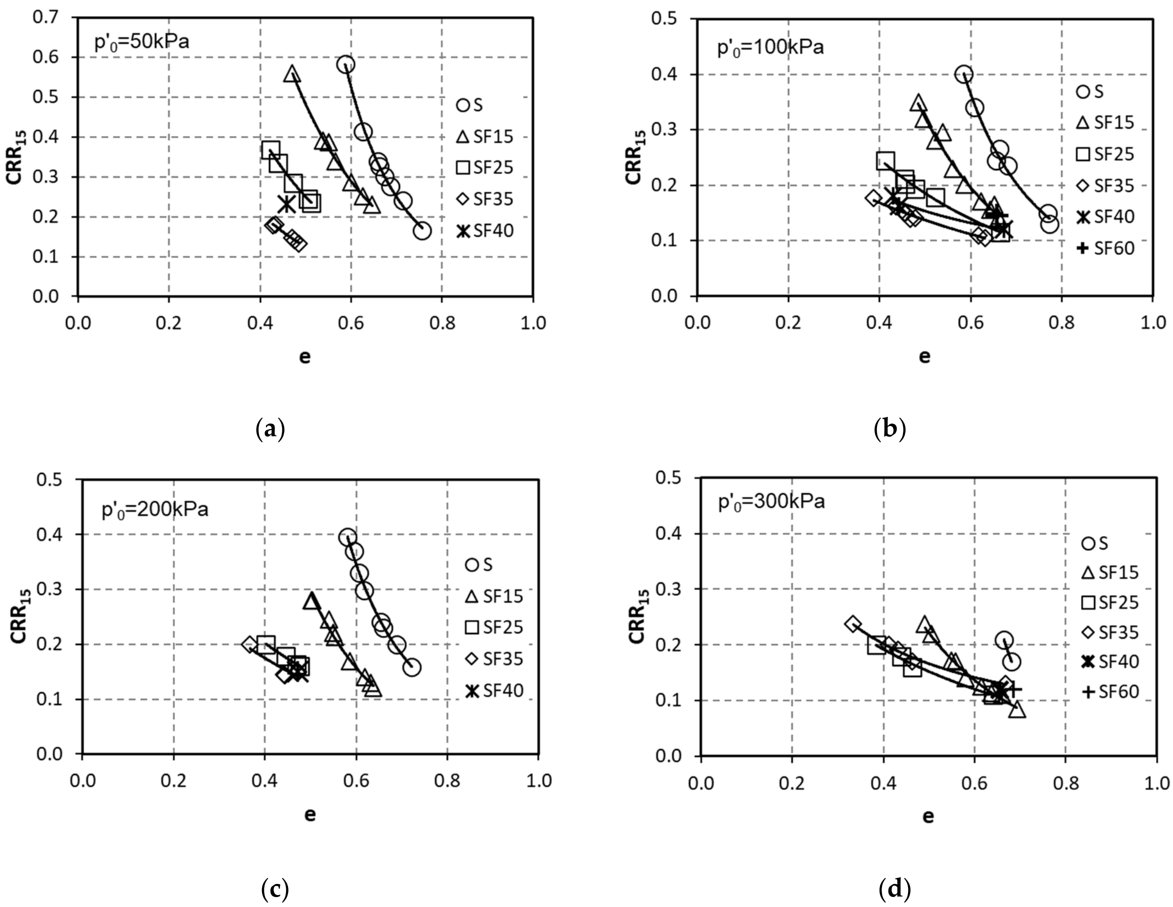

Figure 7. Variation of liquefaction resistance ratio, CRR_{15}, with void ratio, e, for sand and the non-plastic mixtures at the effective stresses, p'_0, (**a**) 50 kPa, (**b**) 100 kPa, (**c**) 200 kPa, (**d**) 300 kPa.

4.3. Correlation of Shear Wave Velocity with Liquefaction Resistance

For each soil type, the measured V_s value at a given p'_0 and density were correlated with CRR_{15}, obtained from the above-described database, Figure 8. To account for the effect of p'_0 on the correlation between CRR_{15} and V_s, V_s was normalized by the stress function, $f(p'_0) = {p'_0}^{m/2}$ in Figure 9, where m is the stress exponent parameter determined for each soil type as described above, Table 4. It is shown in Figure 9, that the CRR_{15}-$V_s/{p'_0}^{m/2}$ curves shift to the left with increasing f_c up to 25% and then start to move downwards and towards the right when f_c is increased to 35%. As noted above for the tested mixtures, $f_{c,th}$ is 35% and 25% at p'_0 = 50–200 kPa and 300 kPa, respectively.

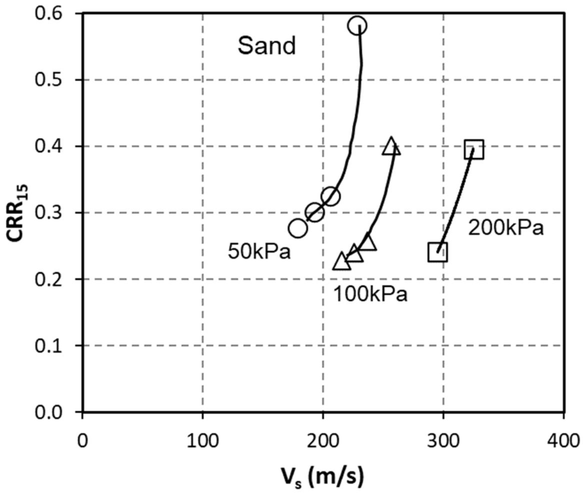

(**a**)

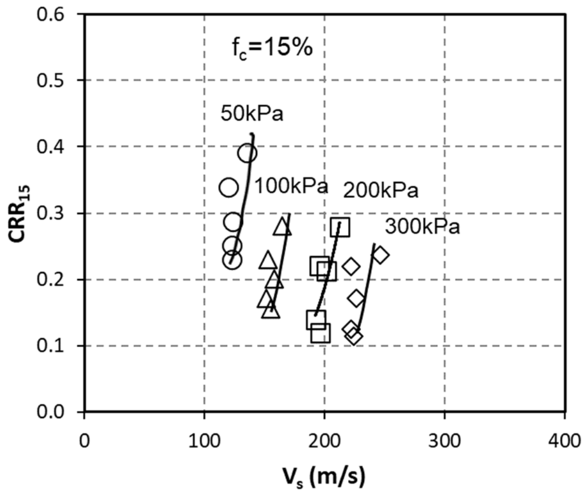

(**b**)

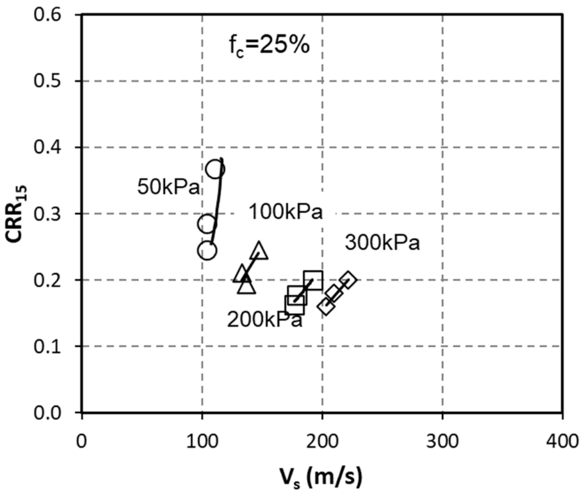

(**c**)

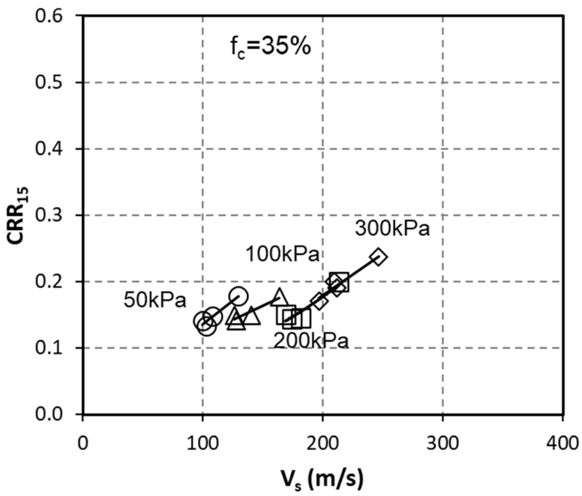

(**d**)

Figure 8. Variation of liquefaction resistance ratio, CRR_{15}, with shear wave velocity, V_s, at various levels of effective stress, p'_0, for: (**a**) sand, (**b**) f_c = 15%, (**c**) f_c = 25% and (**d**) f_c = 35%.

The evaluation of the field CRR_{field}–V_{s1} relationship from the test results of this work requires the conversion of the laboratory CRR_{15} to an equivalent field CRR_{field} and the correction of V_s values for overburden stress. In particular, the laboratory CRR_{15} obtained from unidirectional cyclic triaxial tests on isotropically consolidated specimens should be corrected for the multidirectional character of earthquake loading and the k_0 conditions of lateral earth pressure at rest that exists in the field. Therefore, to convert laboratory CRR_{15} to an equivalent field CRR_{field}, the following correction factors are applied [46]:

$$CRR_{field} = \frac{\tau_l}{\sigma'_v = 100} = r_c \cdot CRR_{15,\sigma'_v=100} = r_c \cdot \frac{CRR_{15,\sigma'_v}}{K_\sigma} = r_c \cdot \frac{c_r}{K_\sigma} \cdot CRR_{15,p'0} \quad (5)$$

where r_c is a factor to consider multidirectional earthquake loading with a value between 0.9 and 1.0, assumed to be 0.90 [46], $K_\sigma = CRR_{15,\sigma'v}/CRR_{15,\sigma'v\,=\,100}$ the overburden stress correction factor and $c_r = (1 + 2 \cdot k_0)/3$ is a factor to convert laboratory CRR_{15}, determined under isotropic conditions, to field k_0 conditions. For the tested materials, the coefficient of lateral earth pressure at rest, k_0, was calculated from $1 - \sin(\varphi'_{cs})$, where φ'_{cs} is the angle of shearing resistance at a critical state, determined from undrained monotonic triaxial tests [45]. The values of k_0, φ'_{cs}, and factor c_r, used for each soil type are presented in Table 5.

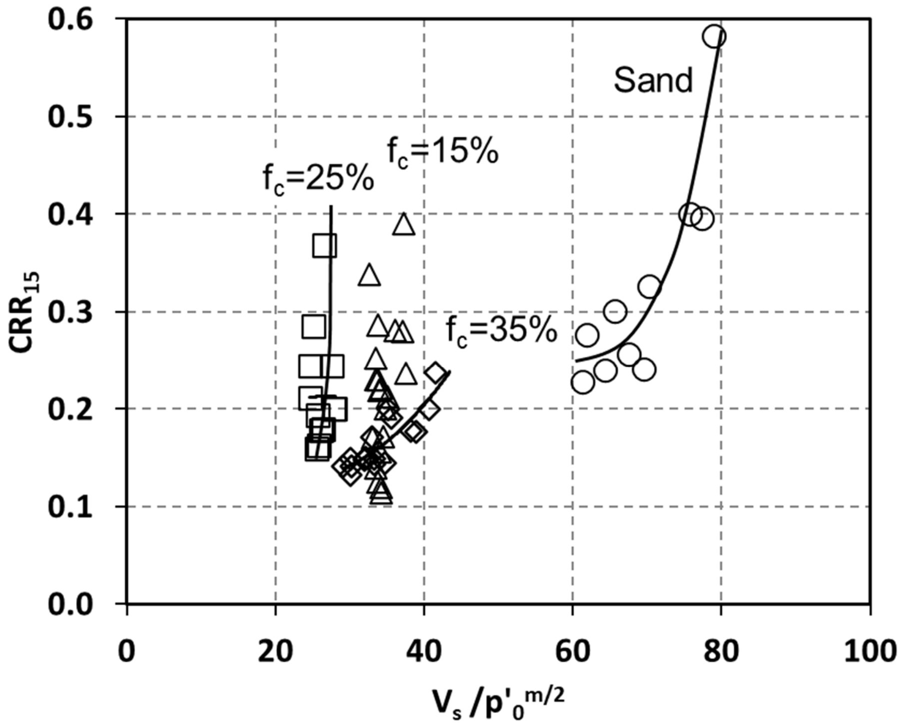

Figure 9. Variation of liquefaction resistance ratio, CRR_{15}, with normalized shear wave velocity, $V_s/p'_0{}^{m/2}$, for the tested soils.

Table 5. Values of k_0 parameter of tested materials.

Soils	φ'_{cs} (°)	k_0	$c_r = (1 + 2k_0)/3$
S	33.56	0.447	0.631
SF15	37.88	0.386	0.591
SF25	34.77	0.430	0.620
SF35	35.47	0.420	0.613

The overburden stress correction factor, K_σ, depends on D_r and soil—reconstituted or undisturbed samples—and test type [47,48]. In this work, K_σ, was derived from the cyclic triaxial tests, conducted on the tested soils [28]. Figure 10a–d present the variation of K_σ with normalized overburden effective stress, $\sigma'_v/100$, at various values of D_r for each soil type. For all soil types and σ'_v below 100 kPa, K_σ increases with decreasing σ'_v at all values of D_r examined. Moreover, for a given σ'_v, lower values of K_σ at higher D_r are in general indicated. However, for σ'_v above 100 kPa, different types of variations of K_σ with σ'_v are observed, depending on f_c. For the sand and the sand–silt mixtures with and 25%, K_σ decreases with increasing $\sigma f_c = 15\%'_v$, with K_σ values becoming smaller with increasing D_r, Figure 10a to c. Moreover, at a given D_r, K_σ values at $f_c = 15\%$ and 25% are lower than the corresponding for the sand. However, for the sand–silt mixture with $f_c = 35\%$ and σ'_v above 100 kPa, K_σ decreases initially and then increases with increasing σ'_v, with K_σ values becoming smaller with increasing D_r, Figure 10d. The minimum K_σ values take place at $\sigma'_v/100$ ratios between 1.70 and 3.4.

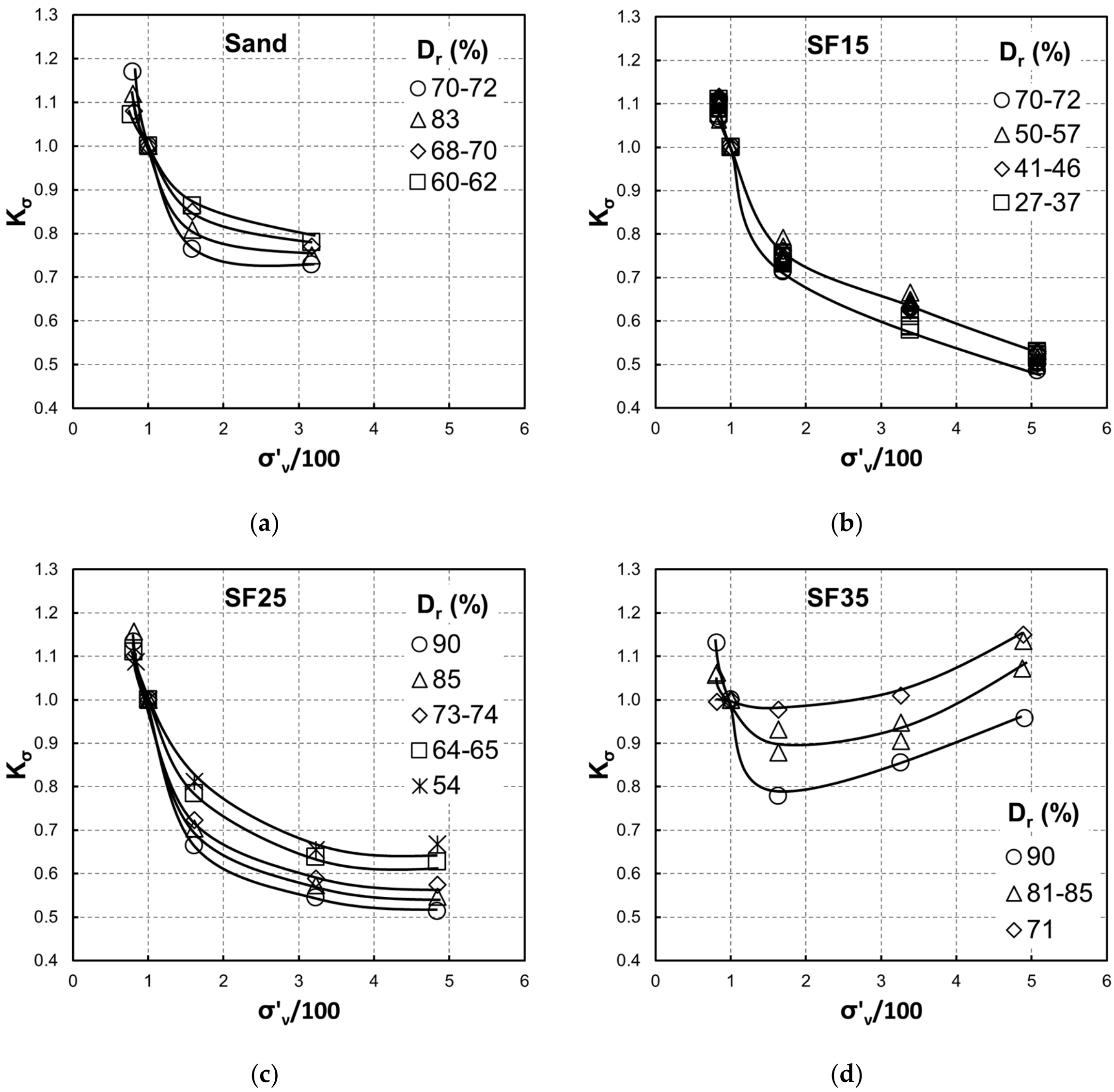

Figure 10. Overburden correction factor, K_σ, versus normalized overburden effective stress, $\sigma'_v/100$ for: (**a**) sand, (**b**) f_c = 15%, (**c**) f_c = 25%, and (**d**) f_c = 35%.

To correct V_s for overburden stress, a factor C_N, as given in Equation (1), is commonly used, similarly to the traditional procedures for modifying standard and cone penetration resistances for overburden stress. Salgado et al. (1997) [49] developed relationships between CPT resistance, relative density, vertical effective stress, and lateral earth pressure coefficient at rest, by means of numerical analyses, and expressed the overburden normalization exponent a in Equation (1) as a function of D_r ($a = b - cD_r$). Boulanger (2003) [48] reevaluated the SPT calibration chamber test data on sand, presented by Marcuson and Bieganousky (1997) [50,51], and expressed the exponent a, also as a function of D_r, ($a = b{\cdot}{D_r}^c$). Both the aforementioned functions correspond to sand.

In this work, the exponent a, of factor C_N was evaluated using two approaches. In the first approach, it was assumed that $a = m/2$, where m is the stress exponent parameter in Equations (3) and (4), Table 4. In the second approach, V_s was expressed as a function of confining stress, p'_0, and D_r, according to the results of bender element tests and the exponent a was expressed as a function of D_r in the form of $b - c{\cdot}D_r$ [49]:

$$V_s = B{\cdot}\left(p'_0\right)^a{\cdot}{D_r}^d = B{\cdot}\left(\frac{(1+2{\cdot}k_0)}{3}\right)^\alpha{\cdot}{\sigma'_v}^a{\cdot}{D_r}^d = B'{\cdot}{\sigma'_v}^{b-c{\cdot}D_r}{\cdot}{D_r}^d \quad (6)$$

Parameters B', b, c, and d, are soil type-dependent properties, obtained from a non-linear regression analysis, and their values are presented in Table 6. Figure 11 shows the variation of exponent a, with D_r for the sand and the sand–silt mixtures. The values of the exponent a are calculated from the bender element tests results using the following equation:

$$a = \frac{\log V_s - \log B' - d \cdot \log D_r}{\log(\sigma'_v)} \tag{7}$$

Table 6. Values of parameters B', b, c, and d in Equation (6) for the tested soils.

Soils	D_r (%)	B'	b	c	Range of a $a = b - c\,D_r$	d	(r^2) *
S	60–100	75.865	0.330	0.076	0.284–0.254	0.731	0.984
SF15	28–70	27.265	0.302	−0.062	0.319–0.345	−0.085	0.983
SF25	54–90	22.678	0.340	−0.036	0.359–0.372	0.135	0.996
SF35	68–100	47.514	0.471	0.208	0.330–0.258	1.828	0.988

* Coefficient of correlation.

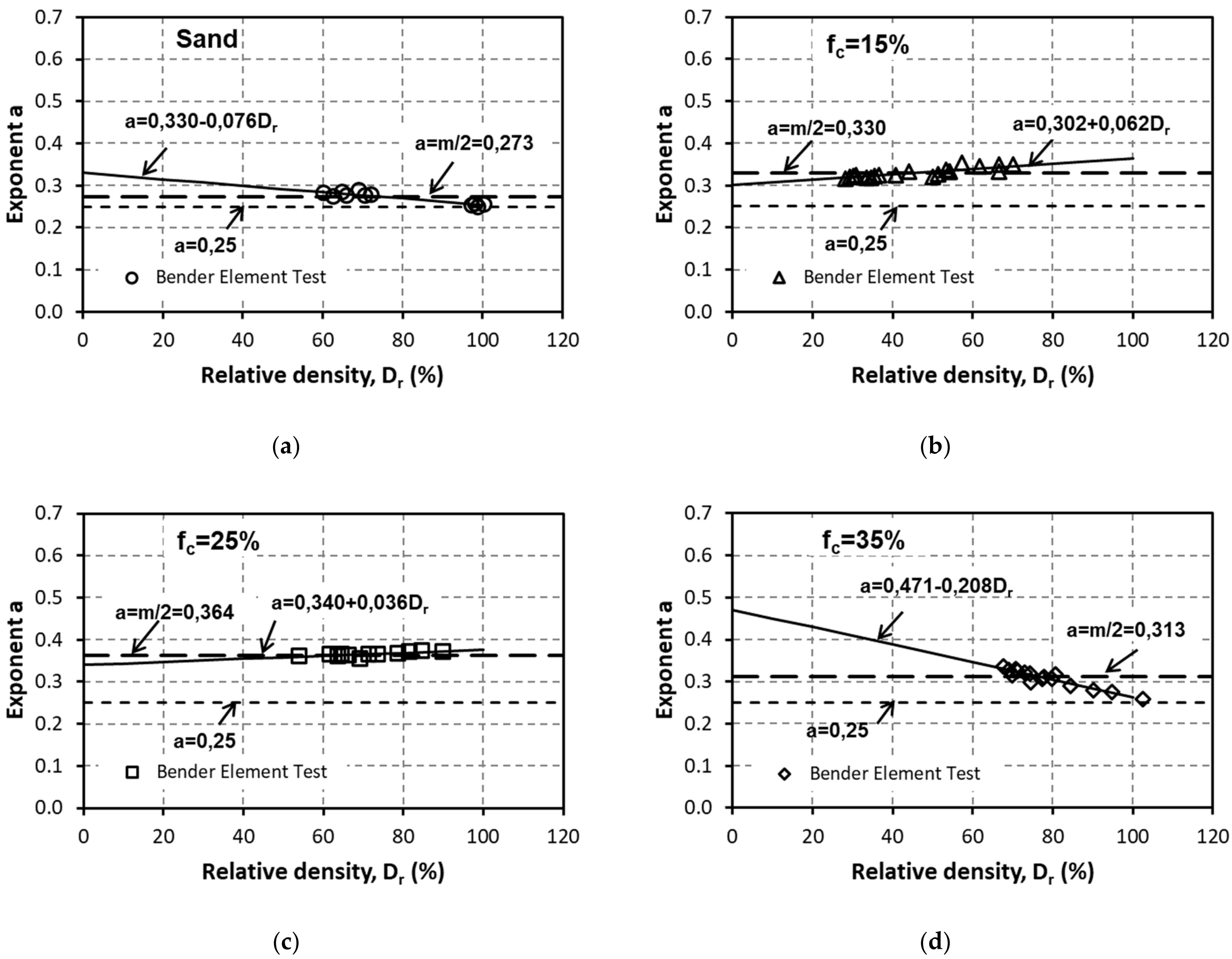

Figure 11. Overburden stress correction exponent, a, versus relative density, D_r, for: (**a**) sand, (**b**) f_c = 15%, (**c**) f_c = 25%, and (**d**) f_c = 35%.

In Figure 11, the values of the exponent a, determined by the second approach, are also compared with the values of a = 0.25 and a = m/2. It is shown that for all tested soils, the range of the values of exponent a, determined by the second approach, is close to the value of a = m/2. In particular, for the sand and the examined range of D_r, the variation of exponent a is from 0.254 to 0.284, Table 6, which may be considered close to the value of 0.25, used commonly for sand. However, for the sand–silt mixtures, higher values of exponent a are anticipated.

Thus, in this work, the overburden stress-corrected shear wave velocity, V_{s1}, is calculated from measured V_s using Equation (1) with a = m/2:

$$V_{s1} = V_s \cdot \left(\frac{p_a}{\sigma'_v}\right)^{\frac{m}{2}} = V_s \cdot \left(\frac{1+2k_0}{3}\right)^{\frac{m}{2}} \cdot \left(\frac{p_a}{p'_0}\right)^{\frac{m}{2}} \quad (8)$$

where p_a is the reference overburden effective stress equal to 100 kPa.

The CRR_{field}–V_{s1} correlations determined for the sand and the sand–silt mixtures are presented in Figure 12, using the proposed stress exponent a = m/2 and the typical stress exponent a = 0.25, for comparison reasons. Similar to the CRR_{15}-$V_s/p'_0{}^{m/2}$, the CRR_{field}–V_{s1} curves move to the left with increasing f_c up to 25% and then downwards and to the right with a further increase of f_c to 35%. In the mixtures with f_c = 15% and 25% there is a significant scatter in the CRR_{field}–V_{s1} curves when a = 0.25 is used. Moreover, there are indications that the liquefaction resistance of these mixtures is underestimated when a = 0.25 is used.

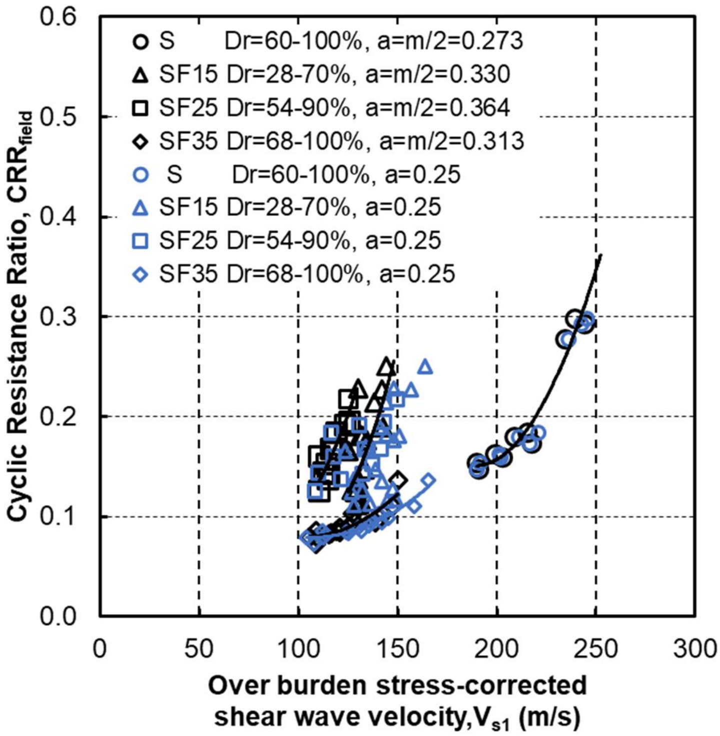

Figure 12. Variation of cyclic resistance ratio, CRR_{field}, with overburden stress corrected shear wave velocity, V_{s1}, for the tested materials.

The results indicate that f_c has a significant influence on the CRR_{field}–V_{s1} correlation and that at the $f_{c,th}$ mixtures are unstable showing the lowest liquefaction resistance values even though they are in a dense state.

Figure 13 presents the CRR_{field}–V_{s1} correlation results determined for the sand, as well as the curves determined for soils with $f_c \leq 5\%$ by previous field and laboratory studies for comparison. The CRR_{field}–V_{s1} results for the sand in this work lay on the curves recommended by [10,11] and to the right of the curves recommended by [5,6,13,14]. The curve suggested by [6] has been drawn as reported by [13] (data analysis from twelve different sand types with f_c = 0–9.6%, D_{60} = 0.167–0.324 mm and C_u = 1.4–2.2 and 15 cycles of loading, assuming e_{min} = 0.65, K_0 = 0.5 and r_c = 0.9). The curve by [13] has been drawn for f_c = 0%, as suggested in their paper. All the data and curves, obtained from previous laboratory studies [15,17–24], lay to the left of the results of this work. This difference may reflect differences in the mineralogy, grain, and grading characteristics of the soils and testing conditions. The maximum estimated V_{s1} value is of the order of 244 m/s at D_r = 100%, as compared to the limiting upper value of 215 m/s, proposed in the semi-empirical procedure and the upper range of values from 177 to 222 m/s, observed for the results of previous laboratory studies.

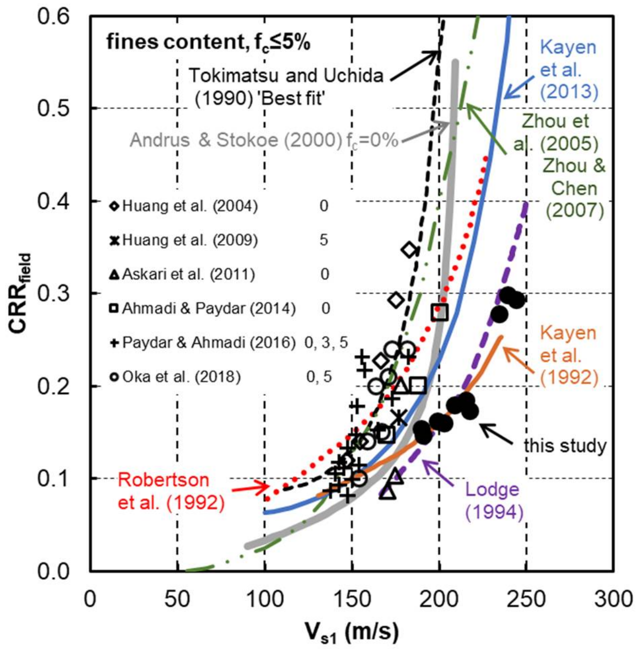

Figure 13. Variation of cyclic resistance ratio, CRR_{field}, with overburden stress corrected shear wave velocity, V_{s1}, for soils with $f_c \leq 5\%$.

Figure 14 presents the CRR_{field}–V_{s1} correlation results determined for the sand–silt mixture with f_c = 15% together with results of previous field and laboratory studies for comparison. The CRR_{field}–V_{s1} correlation data for the sand–silt mixture (D_{50} = 0.30 mm, C_u = 8.8) of this work lay to the left of the curves recommended by all previous field and most laboratory studies [15,21,23], and practically coincide with those reported by [24] for an artificial sand–silt mixture with f_c = 15% and similar grading characteristics (D_{50} = 0.28 mm, C_u = 9.7) and rounded grains. The maximum estimated V_{s1} value is of the order of 144 m/s at D_r = 70%, as compared to the limiting upper value of 204 m/s, proposed in the semi-empirical procedure and the upper range of values from 157 to 181 m/s, observed for the results of previous laboratory studies.

Figure 15 presents the CRR_{field}–V_{s1} correlation results determined for the sand–silt mixture with f_c = 25% together with results of previous field and laboratory studies for comparison. The CRR_{field}–V_{s1} correlation data for the sand–silt mixture of this work lay to the left of the curves recommended by all previous field and laboratory studies. The maximum estimated V_{s1} value is of the order of 126 m/s at D_r = 90%, as compared to the limiting upper value of 200 m/s, proposed in the semi-empirical procedure, and the upper range of values from 160 to 166 m/s, observed for the results of previous laboratory studies.

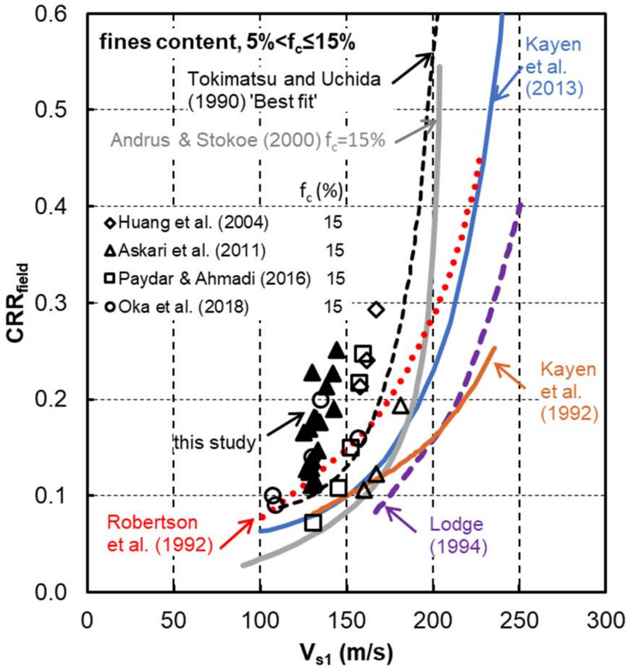

Figure 14. Variation of cyclic resistance ratio, CRR_{field}, with overburden stress corrected shear wave velocity, V_{s1}, for soils with $5 < f_c \leq 15\%$.

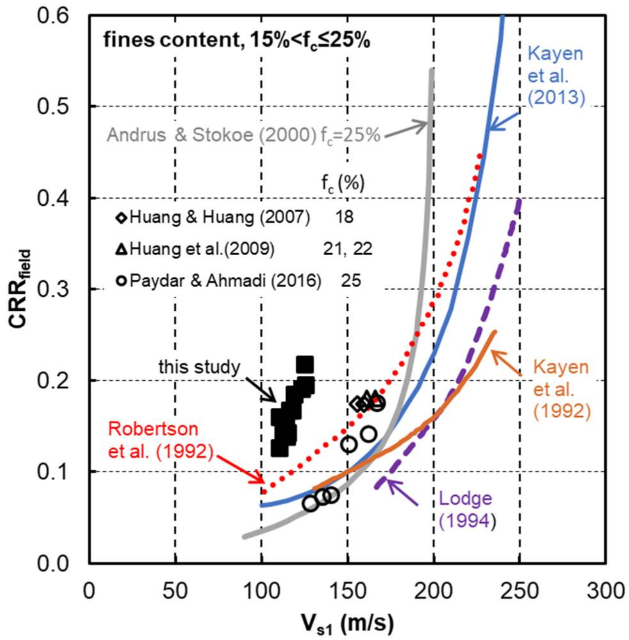

Figure 15. Variation of cyclic resistance ratio, CRR_{field}, with overburden stress corrected shear wave velocity, V_{s1}, for soils with $15 < f_c \leq 25\%$.

Finally, Figure 16 presents the CRR_{field}–V_{s1} correlation results determined for the sand–silt mixture with f_c = 35% together with results of previous field and laboratory studies for comparison. The CRR_{field}–V_{s1} correlation data for the sand–silt mixture of this work (D_{50} = 0.27 mm, C_u = 24.6) lay, again, to the left of the curves recommended by [13] and are in good agreement with the curves of [5,10,14]. They practically coincide with the results reported by [15,21,24] for artificial sand–silt mixtures with f_c = 35% and have similar grading characteristics. The maximum estimated V_{s1} value is of the order of 150 m/s at D_r = 100%, as compared to the limiting upper value of 194 m/s, proposed in the semi-empirical procedure, and the upper range of values from 149 to 171 m/s, observed for the results of previous laboratory studies.

The results from the previously reported field and laboratory studies and the work presented in this paper, indicate that the effect of fines is much more distinct in the case of the laboratory-based CRR_{field}–V_{s1} correlation. Factors contributing to the difference between the field and laboratory-based CRR_{field}–V_{s1} correlation may include stress history, fabric, ageing, and the type of laboratory test used to estimate liquefaction resistance. It is worth noting that grain characteristics of natural silty sand are more complex than that of the artificial sand–silt mixtures with binary packing, as tested in this work and most previous laboratory investigations. Natural sand has an infinite number of particle diameters with varying shape characteristics and may contain particles whose behaviour is dictated by interacting surface forces. Moreover, laboratory tests are element tests, whereas field measurements of V_s may also be affected by soil stratigraphy and boundary conditions.

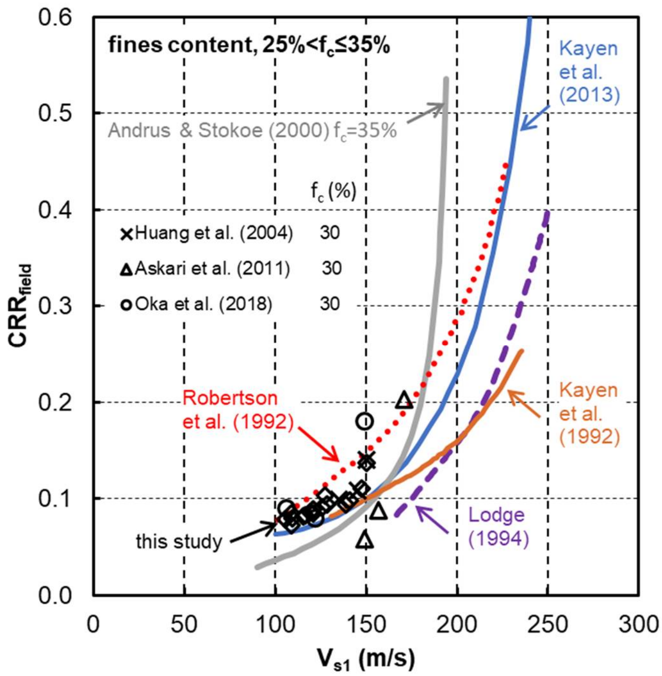

Figure 16. Variation of cyclic resistance ratio, CRR_{field}, with overburden stress corrected shear wave velocity, V_{s1}, for soils with $25 < f_c \leq 35\%$.

5. Conclusions

The following conclusions can be drawn from the results of bender element and cyclic triaxial tests conducted on sand and its mixtures with an NP silt:

(i) The correlation between CRR and V_s of sand containing NP fines depends on factors, such as f_c and p'_0. When V_s is normalized with respect to p'_0, a good correlation between CRR and stress normalized shear waves velocity, $V_s/p'_0{}^{m/2}$, irrespective of stress level is observed. The stress exponent m depends on f_c. The sand–silt mixture with f_c = 35%, forms a lower bound for the CRR_{15}–$V_s/p'_0{}^{m/2}$ correlation;

(ii) The f_c-dependent stress exponent, m/2, can be used in the overburden stress correction of V_s;

(iii) The type of the estimated CRR_{field}–V_{s1} correlation is similar to the correlation between CRR and $V_s/p'_0{}^{m/2}$ and depends significantly on f_c. The sand–silt mixture with f_c = 35% forms the lower bound for this correlation;

(iv) The comparison of derived CRR_{field}–V_{s1} correlation results in this work with previous field and laboratory studies indicates that besides f_c, other factors, such as mineralogy, grain and grading characteristics, fabric, ageing, and stress history may be important.

Author Contributions: Conceptualization, T.M.T.; Investigation, A.I.P. and T.M.T.; Methodology, A.I.P. and T.M.T.; Supervision, T.M.T.; Validation, A.I.P.; Writing—original draft, A.I.P. and T.M.T.; Writing—review & editing, T.M.T. All authors have read and agreed to the published version of the manuscript.

Funding: This research received no external funding.

Institutional Review Board Statement: Not applicable.

Informed Consent Statement: Not applicable.

Data Availability Statement: Data supporting reported results are included in the article and in the first author's PhD thesis, available from the National Documentation Centre at the Greek National Archive of PhD Theses, https://www.didaktorika.gr/eadd/handle/10442/24491?locale=en (accessed on 26 July 2021).

Conflicts of Interest: The authors declare no conflict of interest.

List of Notations

V_s	shear wave velocity
CRR	cyclic resistance ratio or liquefaction resistance
CRR_{lab}	cyclic resistance ratio measured at the laboratory
CRR_{field}	field cyclic stress ratio
V_{s1}	overburden stress-corrected shear wave velocity
f_c	fines content
C_N	factor to correct measured shear wave velocity for overburden stress
p_a	reference stress equal to 100 kPa
σ'_v	effective overburden stress (vertical effective stress)
CSR	cyclic stress ratio equal to $\sigma_d/2p'_0$
D_{50}	mean grain size
D_{10}	diameter corresponding to 10% finer
C_u	coefficient of uniformity
e_{max}	maximum void ratio
e_{min}	minimum void ratio
ε_{DA}	double amplitude axial strain
k_0	coefficient of lateral earth pressure at rest
R_u	excess pore water pressure ratio
CRR_{CTX}	cyclic resistance ratio or liquefaction resistance from cyclic triaxial tests
G_{max}	linear elastic shear modulus
G_s	specific gravity of soil grains
B	degree of saturation, $B = \Delta u/\Delta\sigma$
Δu	excess pore water pressure
f	frequency
p'_0	effective isotropic stress (mean effective stress)-(confining stress)
e	void ratio after consolidation
ρ	total mass density of a soil
CRR_{15}	cyclic resistance ratio or liquefaction resistance at 15 cycles of loading
$\pm\sigma_d$	sinusoidally varying axial stress
N	number of loading cycles
N_l	number of loading cycles at ε_{DA} = 5%
t	Time
A	parameter dependent on soil type
m	parameter dependent on soil type
n	parameter dependent on soil type
D_r	relative density
$f_{c,th}$	threshold fines content
τ_l	cyclic shear strength
r_c	factor to consider multidirectional loading
$CRR_{15,\sigma'v = 100}$	cyclic resistance ratio at 15 cycles of loading and at σ'_v = 100 kPa
$CRR_{15,\sigma'v}$	cyclic resistance ratio at σ'_v
K_σ	correction factor for the level of vertical effective stress

c_r	factor to convert stress ratio to cause liquefaction to field k_o conditions
$CRR_{15,p'0}$	cyclic resistance ratio at 15 cycles of loading and at p'_0
φ'_{cs}	angle of shearing resistance at critical state
B	parameter obtained from a nonlinear regression
B′	parameter obtained from a nonlinear regression
a	parameter obtained from a nonlinear regression
b	parameter obtained from a nonlinear regression
c	parameter obtained from a nonlinear regression
d	parameter obtained from a nonlinear regression
D_{60}	diameter corresponding to 60% finer

References

1. Seed, H.B.; Idriss, I.M. Simplified procedure for evaluating soil liquefaction potential. *J. Soil Mech. Found. Div. ASCE* **1971**, *97*, 1249–1273. [CrossRef]
2. Idriss, I.M. An update to the Seed-Idriss simplified procedure for evaluating liquefaction potential. In Proceedings of the TRB Workshop on New Approaches to Liquefaction, Washington, DC, USA, 10 January 1999.
3. Idriss, I.M.; Boulanger, R.W. Semi-empirical procedures for evaluating liquefaction potential during Earthquakes. In Proceedings of the Joint Eleventh International Conference on Soil Dynamics and Earthquake Engineering and Third International Conference on Earthquake Geotechnical Engineering, Berkeley, CA, USA, 7–9 January 2004; Volume 1, pp. 32–56.
4. Cavallaro, A.; Capilleri, P.; Grasso, S. Site characterization by in situ and laboratory tests for liquefaction potential evaluation during Emilia Romagna earthquake. *Geosciences* **2018**, *8*, 242. [CrossRef]
5. Robertson, P.K.; Woeller, D.J.; Finn, W.D.L. Seismic Cone penetration test for evaluating liquefaction potential under cyclic loading. *Can. Geotech. J.* **1992**, *29*, 686–695. [CrossRef]
6. Tokimatsu, K.; Uchida, A. Correlation between liquefaction resistance and shear wave velocity. *Soils Found.* **1990**, *30*, 33–42. [CrossRef]
7. Tokimatsu, K.; Yamazaki, T.; Yoshimi, Y. Soil liquefaction evaluations by elastic shear moduli. *Soils Found.* **1986**, *26*, 25–35. [CrossRef]
8. Yoshimi, Y.; Tokimatsu, K.; Kaneko, O.; Makihara, Y. Undrained cyclic shear strength of a dense Niigata sand. *Soils Found.* **1984**, *24*, 131–145. [CrossRef]
9. Yoshimi, Y.; Tokimatsu, K.; Hosaka, Y. Evaluation of liquefaction resistance of clean sands based on high-quality undisturbed. *Soils Found.* **1989**, *29*, 93–104. [CrossRef]
10. Kayen, R.E.; Mitchell, J.K.; Seed, R.B.; Lodge, A.; Nishio, S.; Coutinho, R. Evaluation of SPT-, CPT-, and shear wave-based methods for liquefaction potential assessment using Loma Prieta data. In *Proceedings of the Fourth Japan-U.S. Workshop on Earthquake Resistance Design of Life-line Facilities and Countermeasures for Soil Liquefaction*; Technical Report NCEER-92-0019; Hamada, M., O'Rourke, T., Eds.; MCEER: Buffalo, NY, USA, 1992; pp. 177–204.
11. Lodge, A.L. Shear Wave Velocity Measurements for Subsurface Characterization. Ph.D. Thesis, University of California, Berkeley, CA, USA, 1994.
12. Andrus, R.D.; Stokoe, K.H., II. Liquefaction resistance based on shear wave velocity. In *Proceedings of the National Center for Earthquake Engineering Research Workshop on Evaluation of Liquefaction Resistance of Soils*; Technical Report NCEER-97-0022; Youd, T.L., Idriss, I.M., Eds.; MCEER: Buffalo, NY, USA, 1997; pp. 89–128.
13. Andrus, R.D.; Stokoe, K.H., II. Liquefaction resistance of soils from shear-wave velocity. *J. Geotech. Geoenviron. Eng. ASCE* **2000**, *126*, 1015–1025. [CrossRef]
14. Kayen, R.E.; Moss, R.E.S.; Thompson, E.M.; Seed, R.B.; Cetin, K.O.; Der Kiureghian, A.; Tanaka, Y.; Tokimatsu, K. Shear-wave velocity -based probabilistic and deterministic assessment of seismic soil liquefaction potential. *J. Geotech. Geoenviron. Eng. ASCE* **2013**, *139*, 407–419. [CrossRef]
15. Huang, Y.T.; Huang, A.B.; Kuo, Y.C.; Tsai, M.D. A laboratory study on the undrained strength of a silty sand from Central Western Taiwan. *Soil Dyn. Earthq. Eng.* **2004**, *24*, 733–743. [CrossRef]
16. Huang, A.B.; Huang, Y.T. Undisturbed sampling and laboratory shearing tests on a sand with various fines contents. *Soils Found.* **2007**, *47*, 771–781. [CrossRef]
17. Huang, A.B.; Tai, Y.Y.; Lee, F.W.; Huang, Y.T. Field evaluation of the cyclic strength versus cone tip resistance correlation in silty sands. *Soils Found.* **2009**, *49*, 557–568. [CrossRef]
18. Huang, A.B. The Seventh James K. Mitchell Lecture: Characterization of silt/sand soils. In Proceedings of the Fifth International Conference on Geotechnical and Geophysical Site Characterisation, Gold Coast, QLD, Australia, 5–9 September 2016; Volume 1, pp. 3–18.
19. Zhou, Y.G.; Chen, Y.M.; Ke, H. Correlation of liquefaction resistance with shear wave velocity based on laboratory study using bender element. *J. Zhejiang Univ. Sci. A* **2005**, *6*, 805–812. [CrossRef]
20. Zhou, Y.G.; Chen, Y.M. Laboratory investigation on assessing liquefaction resistance of sandy soils by shear wave velocity. *J. Geotech. Geoenviron. Eng. ASCE* **2007**, *133*, 959–972. [CrossRef]

21. Askari, F.; Dabiri, R.; Shafiee, A.; Jafari, M. Liquefaction resistance of sand-silt mixtures using laboratory-based shear wave velocity. *Int. J. Civ. Eng.* **2011**, *9*, 135–144.
22. Ahmadi, M.; Paydar, N. Requirements for soil-specific correlation between shear wave velocity and liquefaction resistance of sands. *Soil Dyn. Earthq. Eng.* **2014**, *57*, 152–163. [CrossRef]
23. Paydar, N.; Ahmadi, M. Correlation of shear wave velocity with liquefaction resistance for silty sand based on laboratory study. In Proceeding of the Fifteenth Asian Regional Conference on Soil Mechanics and Geotechnical Engineering, Fukuoka, Japan, 9–13 November 2016; pp. 794–799.
24. Oka, G.L.; Dewoolkar, M.; Olson, M.S. Comparing laboratory-based liquefaction resistance of a sand with non-plastic fines with shear wave velocity-based field case histories. *Soil Dyn. Earthq. Eng.* **2018**, *113*, 162–173. [CrossRef]
25. Seed, H.B.; Peacock, W.H. The procedure for measuring soil liquefaction characteristics. *J. Soil Mech. Found. Div.* **1971**, *97*, 1099–1119. [CrossRef]
26. Finn, W.D.L.; Pickering, D.J.; Bransby, P.L. Sand liquefaction in triaxial and simple shear tests. *J. Soil Mech. Found. Div.* **1971**, *97*, 639–659. [CrossRef]
27. Castro, G. Liquefaction and cyclic mobility of saturated sands. *J. Geotech. Eng. Div.* **1976**, *101*, 551–569. [CrossRef]
28. Papadopoulou, A.I. Laboratory investigation into the behavior of silty sands under monotonic and cyclic loading. Ph.D. Thesis, Aristotle University of Thessaloniki, Thessaloniki, Greece, 2008.
29. Ladd, S. Preparing test specimens using undercompaction. *Geotech. Test. J.* **1978**, *1*, 16–23.
30. Verdugo, R.; Ishihara, K. The steady state of sandy soils. *Soils Found.* **1996**, *36*, 81–91. [CrossRef]
31. Theopoulos, A.; Papadopoulou, A.; Th, T. An automated system for measurement of shear waves velocity in soil. In Proceedings of the XIX IMEKO World Congress Fundamental Applied Metrology, Lisbon, Portugal, 6–11 September 2009; pp. 1597–1600.
32. Kawaguchi, T.; Mitachi, T.; Shibuya, S. Evaluation of shear wave travel time in laboratory bender element test. In Proceedings of the Fifteenth International Conference on Soil Mechanics and Geotechnical Engineering, Istanbul, Turkey, 27 August 2001; pp. 155–158.
33. Brignoli, E.G.M.; Gotti, M.; Stokoe, K.H., II. Measurement of shear waves in laboratory specimens by means of piezoelectric transducers. *Geotech. Test. J.* **1996**, *19*, 384–397.
34. Lee, J.S.; Santamarina, J.C. Bender Elements: Performance and Signal Interpretation. *J. Geotech. Geoenviron. Eng. ASCE* **2005**, *131*, 1063–1070. [CrossRef]
35. Ishihara, K. Liquefaction and flow failure during earthquakes. *Géotechnique* **1993**, *43*, 351–415. [CrossRef]
36. Hardin, B.O.; Richart, F.E., Jr. Elastic wave velocities in granular soils. *J. Soil Mechan. Found. Div. ASCE* **1963**, *89*, 33–65. [CrossRef]
37. Jamiolkowski, M.; Leroueil, S.; Lo Presti, D.C.F. Design parameters from theory to practice. In Proceedings of the International Conference on Geotechnical Engineering for Coastal Development, GEO-COAST'91, Yokahama, Japan, 3–6 September 1991; pp. 877–917.
38. Thevanayagam, S. Effect of fines and confining stress on steady state strength of silty sands. *J. Geotech. Eng. ASCE* **1998**, *124*, 479–491. [CrossRef]
39. Polito, C.P.; Martin, J.R. Effects of nonplastic fines on the liquefaction resistance of sands. *J. Geotech. Geoenviron. Eng. ASCE* **2001**, *127*, 408–415. [CrossRef]
40. Naeini, S.A.; Baziar, M.H. Effect of fines content on steady-state strength of mixed and layered samples of a sand. *Soil Dyn. Earthq. Eng.* **2004**, *24*, 181–187. [CrossRef]
41. Yang, S.; Sandven, R.; Grande, L. Steady-state lines of sand-silt mixtures. *Can. Geotech. J.* **2006**, *43*, 1213–1219. [CrossRef]
42. Dash, H.K.; Sitharam, T.G. Undrained cyclic and monotonic strength of sand-silt mixtures. *J. Geotech. Geoenviron. Eng. ASCE* **2011**, *29*, 555–570. [CrossRef]
43. Hsiao, D.H.; Phan, V.T.A. Evaluation of static and dynamic properties of sand-fines mixtures through the state and equivalent state parameters. *Soil Dyn. Earthq. Eng.* **2016**, *84*, 134–144. [CrossRef]
44. Porcino, D.D.; Diano, V.; Triantafyllidis, T.; Wichtmann, T. Predicting undrained static response of sand with non-plastic fines in terms of equivalent granular state parameter. *Acta Geotech.* **2019**, *15*, 867–882. [CrossRef]
45. Papadopoulou, A.; Tika, T. The effect of fines on critical state and liquefaction resistance characteristics of nonplastic silty sands. *Soils Found.* **2008**, *48*, 713–726. [CrossRef]
46. Seed, H.B. Soil liquefaction and cyclic mobility evaluation for level ground during earthquakes. *J. Geotech. Geoenviron. Eng. ASCE* **1979**, *105*, 201–255.
47. Vaid, P.Y.; Sivathayalan, S. Static and cyclic liquefaction potential of Fraser Delta sand in simple shear and triaxial tests. *Can. Geotech. J.* **1996**, *33*, 281–289. [CrossRef]
48. Boulanger, R.W. High overburden stress effects in liquefaction analyses. *J. Geotech. Geoenviron. Eng. ASCE* **2003**, *129*, 1071–1082. [CrossRef]
49. Salgado, R.; Boulanger, R.W.; Mitchell, J.K. Lateral stress effects on CPT liquefaction resistance correlations. *J. Geotech. Geoenviron. Eng. ASCE* **1997**, *123*, 726–735. [CrossRef]
50. Marcuson, W.F., III; Bieganousky, W.A. Laboratory standard penetration tests on fine sands. *J. Geotech. Eng. Div. ASCE* **1997**, *103*, 565–588. [CrossRef]
51. Marcuson, W.F., III; Bieganousky, W.A. SPT and relative density in coarse sands. *J. Geotech. Eng. Div. ASCE* **1997**, *103*, 1295–1309. [CrossRef]